International Journal of Mathematical, Engineering and Management Sciences
Vol. 7, No. 2, 196-210, 2022
https://doi.org/10.33889/IJMEMS.2022.7.2.013

Time Domain Implementation of Consistent Boundaries for Continuum Two-Dimensional Wave Propagation Problems Using ABAQUS User-Defined Elements

J. Rama Raju Patchamatla
Department of Civil Engineering,
Graphic Era (Deemed to be University), Dehradun, Uttarakhand, India.
E.mail: pjramarajufce@geu.ac.in

P. K. Emani
Department of Civil Engineering,
Graphic Era (Deemed to be University), Dehradun, Uttarakhand, India.
Corresponding author: dr.emani.ce@geu.ac.in

(Received on December 12, 2021; Accepted on February 13, 2022)

Abstract
The present paper details the finite element implementation procedure for applying consistent boundaries for two-dimensional continuum soil-structure interaction systems. Consistent boundary conditions are ensured by applying rigorously calculated interaction forces at the truncated soil-structure interface. These calculations involve the evaluation of convolution integral on acceleration unit-impulse response functions for all boundary degrees of freedom for all time steps. The interactive or run-time evaluation of the interaction forces based on the past response history, is successfully carried out using user-defined element formulation in ABAQUS. This precise implementation of this boundary element procedure is demonstrated through benchmark problems and demonstrated through typical stress-wave propagation problems.

Keywords- Consistent boundaries, Wave propagation in soils, Boundary element method, ABAQUS, UEL subroutine.

1. Introduction

The principal problem in dynamic soil-structure interaction (SSI) analysis of continuum domains is the modelling of the boundaries. The semi-infinite soil has to be invariably truncated at a place from where the response is not of interest and beyond which the response is bound to be linear. Such truncated interfaces are typically modelled by viscous dampers that can transmit only the stress waves that impinge normally. Other simple boundaries are local in nature and cannot model the true transparent nature of the site conditions. In discrete domains where the wave dynamics is not modelled, the reflection of stress waves is not an issue (Patchamatla & Emani, 2020; Wolf & Deeks, 2004). For continuum modelling of soil-structure systems, consistent boundaries are suggested by researchers that are founded on wave-dynamic based boundary element formulations, the dynamic implementation of which are quite intricate. In the frequency domain, these consistent boundaries are elegantly implemented through the application of the dynamic stiffness matrix of the truncated domain to the near-field (Emani et al., 2016; Emani & Maheshwari, 2009; Maheshwari & Emani, 2015). In the case of time domain problems, like wave propagation through continuum semi-infinite domains, the use of Artificial Boundary Conditions (ABCs) like in Ni et al. (2022) or the use of Multi-transmitting Formula (MTF) in Spectral element formulation (Xing et al., 2021) is required to ensure transmissibility of the stress waves. Alternatively, the consistent boundaries are applied through the use of acceleration unit-impulse response matrices in time-domain. These boundaries are rigorous, and require large computational effort, involving the full response history till that time step. This requires

the use of state-of-art finite element solvers with advanced user-defined formulations to customize the finite element procedure so as to process the boundary elements, as done by Poul and Zerva (2018).

In the present work, similarity-based boundary finite element method known as Consistent Infinitesimal Finite Element Cell Method (CIFECM) is used to characterize the dynamics of the soil that is truncated from modelling (i.e. the far-field). This method is also referred to as Scaled Boundary Finite Element Method, by emphasizing the method of achieving the consistent boundary formulation (Wolf, 2003). According to Song and Wolf (2000), this method does not require a fundamental solution. In addition, this method reduces the size of a 3D problem to 2D, and of 2D problem to 1D. Further, the method exactly fulfills the radiation boundary condition of unbounded domains, and can accommodate anisotropy of materials (Song & Wolf, 2000). The method has application in a wide variety of applications ranging from structural plate bending problems (Man et al., 2012), crack propagation problems (Yang, 2006), image-based stress analysis (Saputra et al., 2017) to electrostatic (Liu & Lin, 2012) and acoustic problems (Lehmann et al., 2006). For time domain implementation of the consistent boundary conditions, the use of acceleration unit-impulse response functions is recommended (Chen et al., 2014; Lin et al., 2016).

The classical finite element modelling is used for the near-field soil containing the structure and other forms of inhomogeneity. The dynamically-calculated 'soil-structure interaction forces' provide the link between the 'CIFECM of far-field' and the 'FEM of near-field'. This involves interactive calculation and application of forces at all the degrees of freedom of the soil-structure interface. In general-purpose finite element software like ABAQUS, ANSYS, ADINA, the interactive application of loads is possible through user-defined functions or subroutines.

2. Formulation of CIFECM for Acceleration Unit Impulse Response

The similarity based boundary element method is formulated by Wolf and Song (1996). This involves the following steps for two-dimensional displacement field problems:

(i). Creation of Finite Element mesh for near-field (Figure 1).
(ii). Extraction of the nodes at the interface of near-field and far-field i.e., the soil-structure interface (shown in Figure 2).

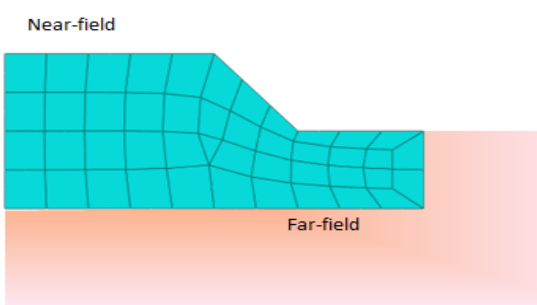

Figure 1. Near- and far-fields of SSI system.

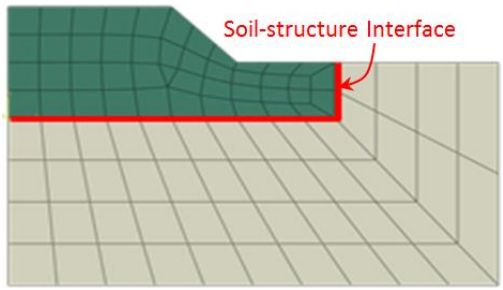

Figure 2. Soil-structure interface/boundary.

(iii). Creating line elements connecting the boundary nodes as two-noded or three-noded boundary elements.
(iv). Generating coefficient matrices for the two-noded boundary elements Eq. (8).

(v). Assembling the coefficient matrices of the two-noded boundary elements.

(vi). Solving the time discretised form of equation of motion, which is referred to as Consistent Infinitesimal Finite Element Cell Equation (CIFEC Equation) for the first time step. Eq. (12). This gives the acceleration unit impulse response function $[m^{\infty}]_1$ for all boundary degrees of freedom for step1.

(vii). Solving the time stepping equation Eq. (15) for subsequent steps to get the acceleration unit-impulse response functions $[m^{\infty}]_n$ for all boundary degrees of freedom for subsequent steps ($n \geq 2$).

(viii). The actual acceleration unit impulse response matrix is the transformed form of $[m^{\infty}]_n$ as given below (for any value of n).

$$[M^{\infty}] = [U]^T [m^{\infty}][U] \tag{1}$$

The formulations used in the above steps are included in the Appendix- A, B. After completion of the above procedure, all the acceleration unit-impulse response functions of all boundary degrees of freedom for all time steps are obtained. The above matrices are all written to external data files to be used in the latter part of the analysis. A typical plot of acceleration unit-impulse response for a degree of freedom is shown in (Figure 3).

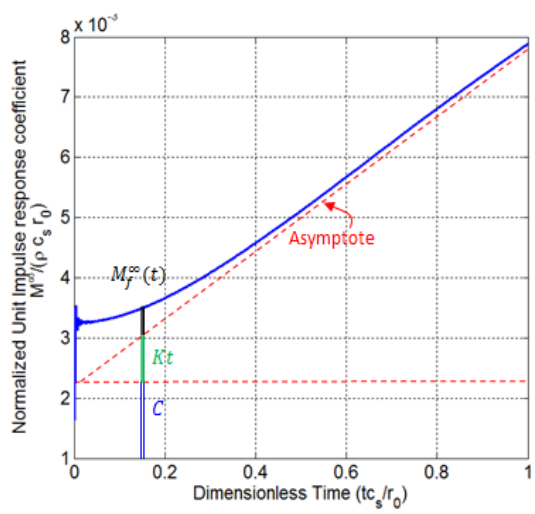

Figure 3. Typical acceleration unit-impulse response function.

In the above procedure, the time discretization and the spatial discretization of boundary should be the same as used for modelling of near-field analysis.

3. Formulation of Soil-Structure Interaction Forces

The consistent boundaries that can effectively absorb all stress waves in all directions can be implemented through the soil-structure interaction forces calculated using the convolution integral given below

$$\{R_b(t)\} = \int_0^t [M_{bb}{}^{\infty}(t-\tau)]\{\ddot{u}_b(t)\}d\tau \tag{2}$$

Where $\{R_b(t)\}$ is the SSI force vector to be applied at SSI, $[M_{bb}{}^{\infty}(t)]$is the acceleration unit-impulse response function in time domain, and $\{\ddot{u}_b(t)\}$ is the acceleration vector of the boundary DOFs at SSI. The evaluation of the discretized form of $[M_{bb}{}^{\infty}(t)]$ is already discussed in the previous section.

In time-discretized form, the above equation can be written at current step n as

$$\{R_b\}_n = \sum_{i=1}^{n} [M_{bb}{}^{\infty}]_{n-i}\{\ddot{u}_b\}_i \Delta\tau \tag{3}$$

Since, the acceleration vector till $n-1$(previous to current) is known, while the acceleration of the current step is to be determined, the above force vector can be split into known and unknown terms as follows

$$\{R_b\}_n = \sum_{i=1}^{n-1} [M_{bb}{}^{\infty}]_{n-i}\{\ddot{u}_b\}_i \Delta\tau + [M_{bb}{}^{\infty}]_0\{\ddot{u}_b\}_n \tag{4}$$

Where $[M_{bb}{}^{\infty}]_0$ is the acceleration unit-impulse response at the first time step, which can be shown to be equal to dashpot matrix $[c^{\infty}]$ (Wolf & Song, 1996). The $[c^{\infty}]$ matrix can be obtained by simple momentum conservation principle applied on the boundary to convert the continuous dashpot function into discrete $[c^{\infty}]$ matrix. Alternatively, the acceleration unit-impulse response can also be resolved into a constant value$[c]$, a linearly varying component$[K]$, an asymptotic component$\left[M_f^{\infty}(t)\right]$, as shown in the Figure 3.

The acceleration unit impulse response matrices $[M_{bb}^{\infty}]_n$ corresponding to the predetermined spatial discretization can be determined for all time steps ($n = 1,2,..N$) before starting the near-field dynamic analysis. This advantage of uncoupling the near-field and far-field analyses is provided by the substructure method both in time domain and frequency domain.

4. Application of SSI Forces Using UEL Subroutine

Implicit dynamic analysis of the near-field is carried out in ABAQUS. The near-field is modelled in ABAQUS as a finite element assembly. The input file is created by the ABAQUS job. A User-defined element containing all the boundary nodes is defined in the input file using *USER ELEMENT and *ELEMENT commands. A FORTRAN95 subroutine UEL( ) is prepared to evaluate the interaction forces in each step. This subroutine follows the steps given below:

(i). Reading the data of acceleration unit impulse response functions of the boundary degrees of freedom into the COMMON block of the UEL subroutine using the UEXTERNALDB subroutine.

(ii). The mass matrix of the boundary element is modified to add the $[M_{bb}{}^{\infty}]_0$ matrix to the mass matrix of the total soil-structure system. This is done at the beginning of the time stepping procedure.

(iii). RHS array is a predefined variable used by UEL( ) subroutine to store the effect of user-defined element on the right-hand side of equations of motion or dynamic equilibrium equations. AMATRX is also a predefined variable used to modify the system coefficient matrices, viz., stiffness, damping and mass matrices. In this step, the RHS and AMATRX variables are initialized to zeros.

(iv). Copying the accelerations of the element degrees of freedom in the current step, into the state variable SVARS.

(v). Evaluating the convolution integral for interaction forces by looping over all the previous time steps.

(vi). Filling the RHS matrix with the interaction force vector for the next time step.

It can be noted that the damping and stiffness matrices of the near-field assembly are not altered in UEL( ) subroutine.

5. Benchmark Problem

5.1 Semi-Infinite Segmental Cavity

The boundary element method is classically tested on cavity walls in one-, two-and three-dimensional problems. For the continuum elements presented in the previous section, the behaviour of a semi-infinite segmental cavity (Figure 4) subjected to a triangular displacement pulse is presented. The semi-infinite medium surrounding the cavity is defined by the properties: Modulus of Elasticity, E, Shear modulus, G, Poisson's ratio, ν, mass density, ρ.

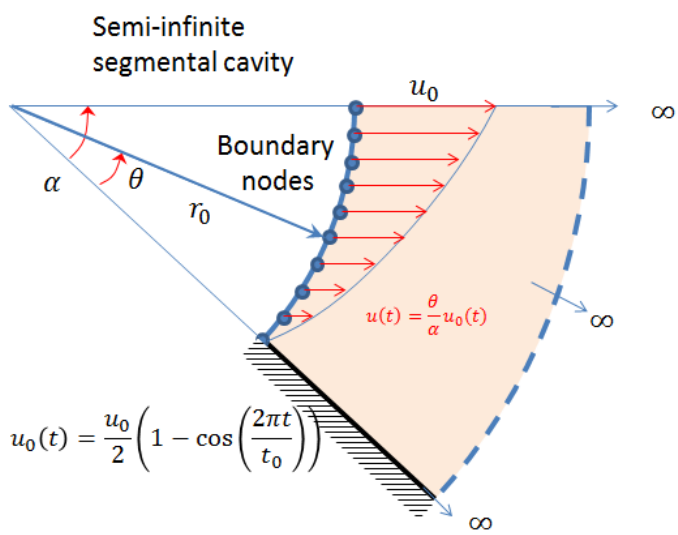

Figure 4. Semi- infinite segmental cavity in two-dimensions.

The triangular displacement pulse has the spatial and temporal distribution given by Eq. (5) (Figure 5).

$$u(t) = \frac{\theta}{\alpha} u_0(t) \tag{5}$$

$$u_0(t) = \frac{u_0}{2}\left[1 - \cos\left(\frac{2\pi t}{t_0}\right)\right] \quad 0 \le t \le t_0 = 1.5\frac{r_0}{c_s} = 1.5\bar{t}$$
$$= 0 \qquad t > t_0 \tag{6}$$

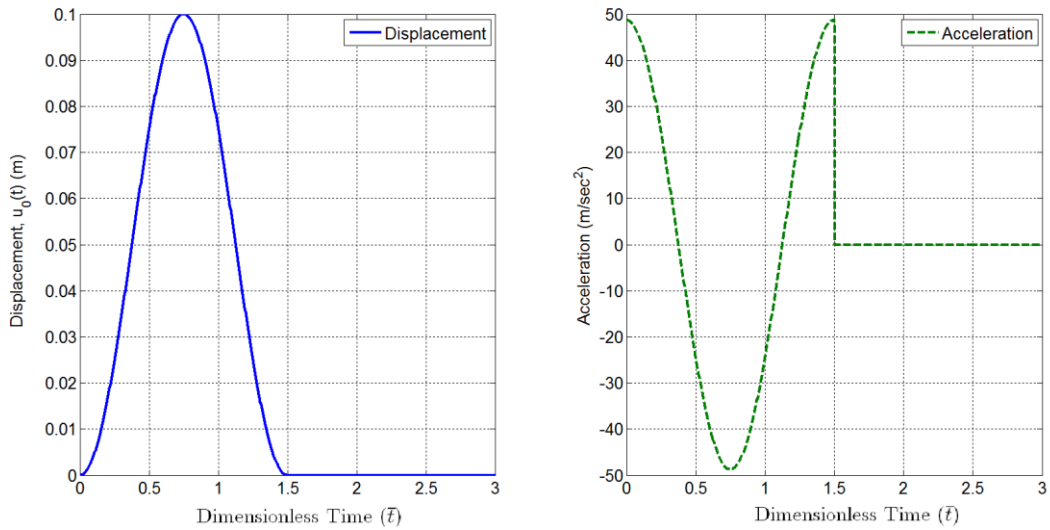

Figure 5. Input Displacement and acceleration time histories.

The time (t) is non-dimensionalized $(\bar{t})$ by normalizing it with the time taken for the shear wave to travel the characteristic length (r_0) i.e., r_0/c_s. For this problem, the characteristic length r_0 is taken as the radius of the cavity, and the velocity of the (shear) stress wave is given by Eq. (7).

$$c_s = \sqrt{\frac{G}{\rho}} \tag{7}$$

The reaction history of the semi-infinite domain to this force pulse is condensed into a single equivalent reaction value at the top of the cavity wall (Figure 6). For this the reactions of all DOF are integrated over the cavity wall taking the spatial distribution of input displacement as weighing function. The reaction history thus obtained is shown in Figure 7. The results published for various other types of boundaries are also shown in Figure 7. It can be seen that the comparison with extended mesh results is perfect till $\bar{t} = 1.5$. The extended mesh results are accepted as standard results.

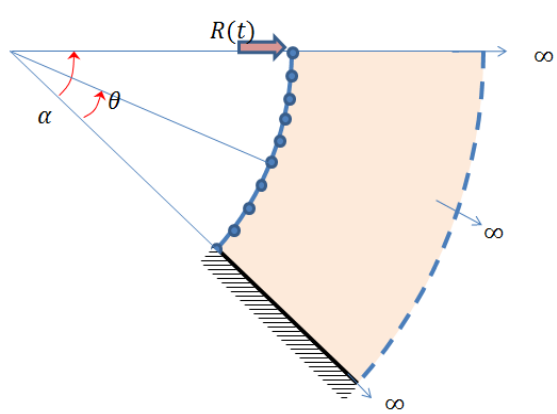

Figure 6. Reaction force $R(t)$ equivalent to SSI reactions.

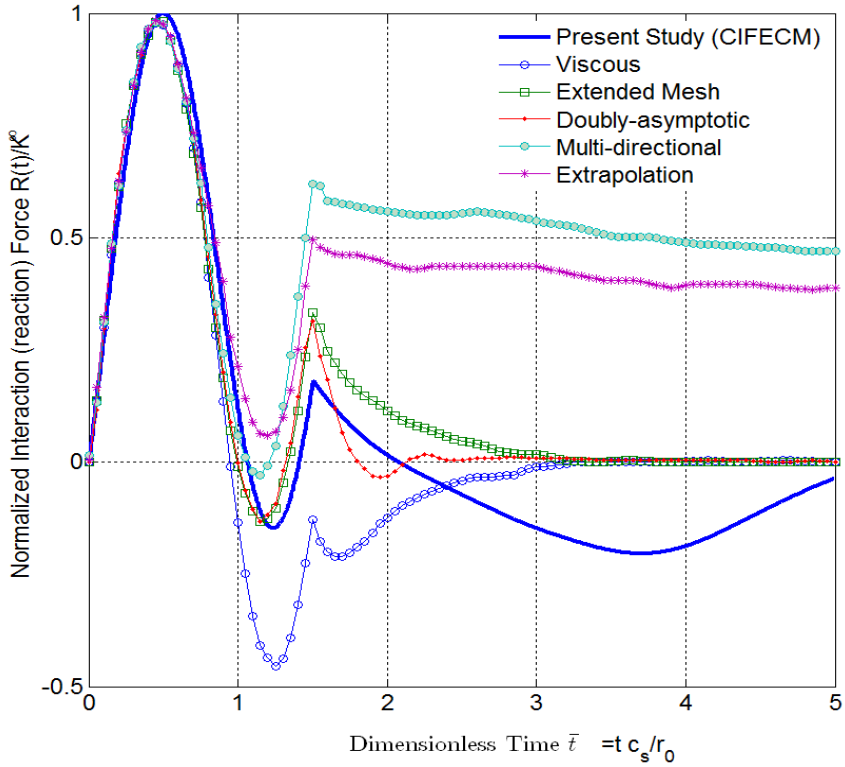

Figure 7. The time history of the reaction force R(t) at the top node.

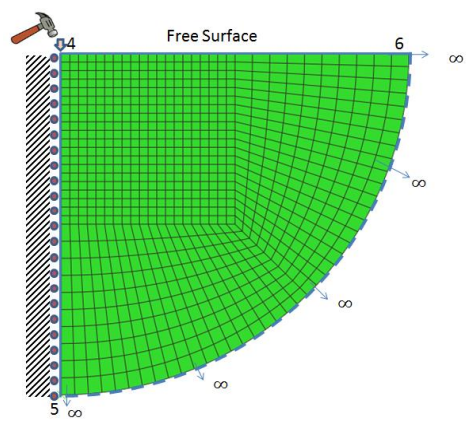

Figure 8. Quarter circular FE model of semi-infinite domain subjected to triangular impact load.

6. Simulation of SASW Test

In this section, the consistent boundaries are used to numerically simulate the Spectral Analysis of Surface Wave (SASW) test. SASW test is a popular field test that uses surface waves to define the shear wave velocity profiles in soil deposits. Elastic waves propagating in the half-space due

to a vertical impact loading is experimentally studied in SASW test. The times responses obtained at a series of stations are recorded so as to get the depth of various underlying soil layers. The responses from a typical SASW test is a result of complex interaction of body and surface waves.

Figure 8 shows the FE model of a semi-infinite soil domain used to simulate the response from SASW test. The model is a half-model of the domain, using symmetric boundary conditions along the axis of symmetry. The vertical impact in the form of triangular pulse (Figure 5) is applied at the free surface. The point of loading is indicated by the node number 4. The responses are presented at nodes 4, 5 and 6 which are also shown in (Figure 8).

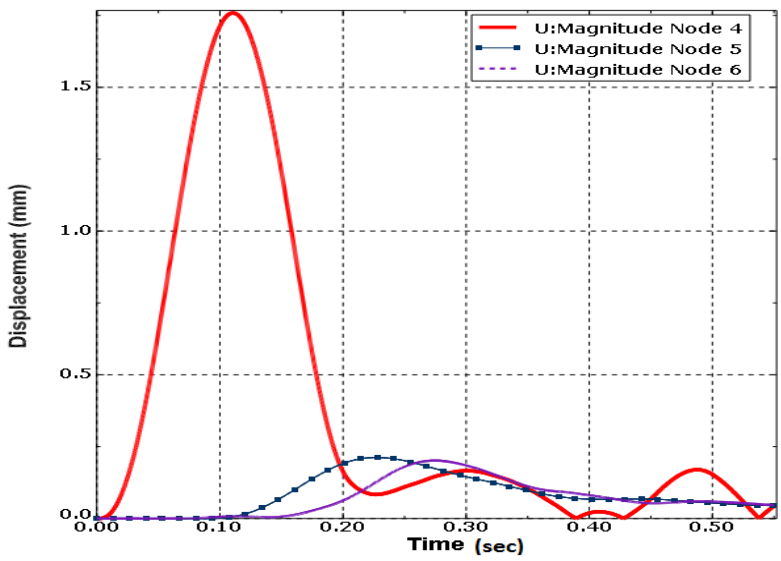

Figure 9. Numerical simulation results of SASW test using quarter circular soil medium.

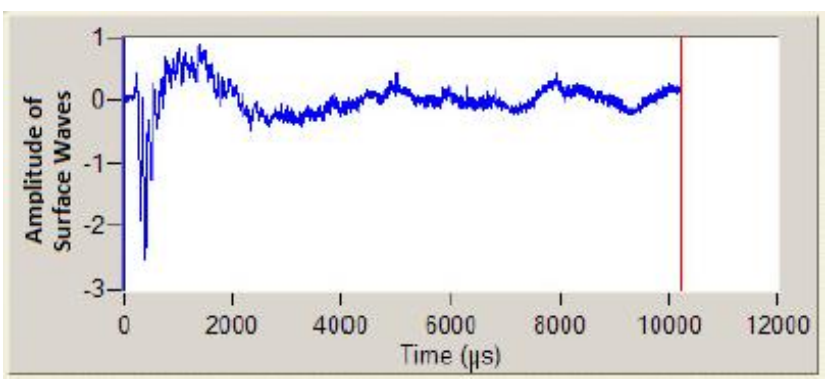

Figure 10. Typical time histories from SASW test (Olsoninstruments, 2021).

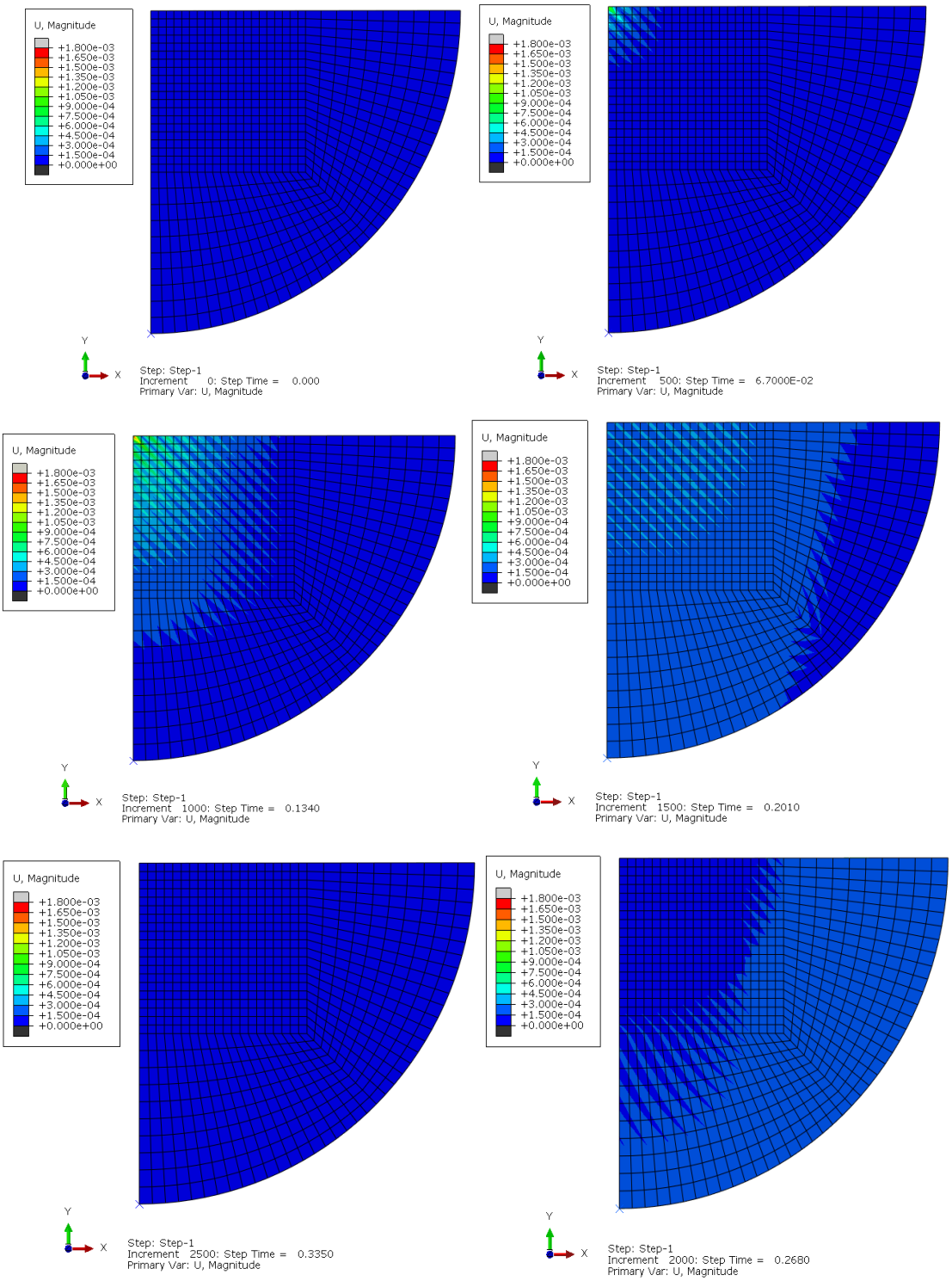

Figure 11. Snapshots of displacement contours showing the wave propagation.

The responses at nodes 4, 5 and 6 are presented (Figure 9), along with the typical results from SASW test (Figure 10). The similarity in the two plots validates the simulation of complex interactions between the body waves and the surface waves. The presence of free surface, causes the surface waves to form, which tend to travel along the free surface (Gucunski & Woods, 1992). On the other hand, the body waves (P-wave) tend to travel into the infinite domain, vertically. With time, there will be interference between these two waves leading to appearance of displacements even after the primary impulse has passed through the modelled domain.

To demonstrate the transmission of stress waves through the SSI without getting reflected back into the model, the snapshots of the displacement wave propagation is given in (Figure 10). It can be observed that the wave front first reaches the SSI boundary along the vertical direction, as can be seen at 0.2 sec. This is the body wave (P-wave) that travels faster in the soil medium. The wave front that reaches the SSI along the horizontal direction (along the free surface) is the surface wave. It can be observed that the surface wave travels slower than the body wave.

For further demonstration of the working of the consistent boundaries in transmitting the stress waves, without reflecting, the snapshots of the stress contours are presented in Figure 11 and Figure 12. Although the domain fell silent at 0.335 sec (Figure 11), the continued silence is shown in Figure 12 for another 0.13 sec. Thus, the user-defined UEL boundary elements are applying appropriate interaction forces so as to transmit the stress waves without reflecting back.

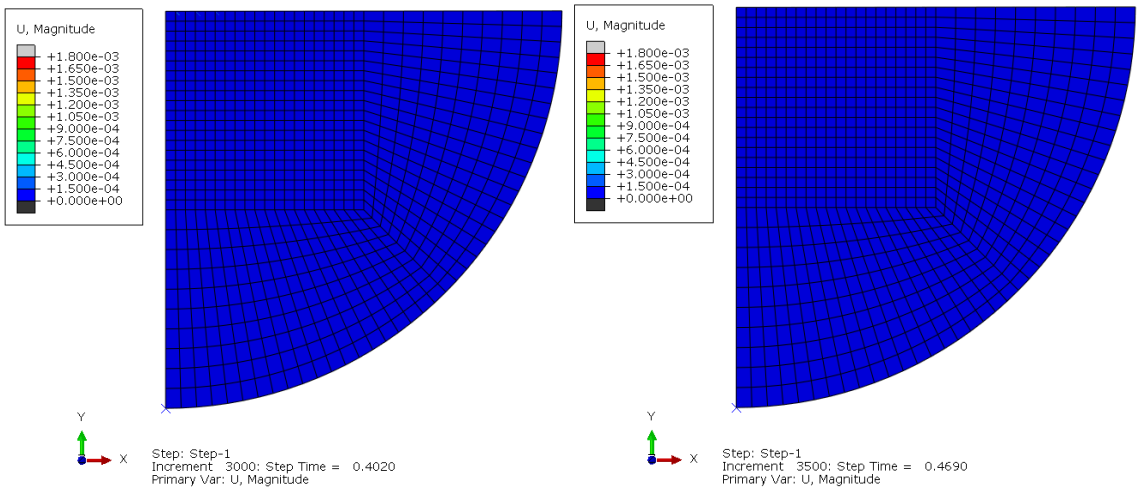

Figure 12. Displacement contours after the wave passed out of the domain.

7. Conclusion

A benchmark problem of semi-infinite wedge cavity is presented to demonstrate the successful implementation of consistent boundaries (CIFECM boundaries) for two-dimensional continuum models under stress wave propagation. This is followed by the presentation of the simulation of wave propagation during SASW test. The waves generated in a SASW test includes both the body and surface waves. Their passing away from the near-field domain into the infinite domain is illustrated through displacement contour plots. The results validate the procedure for

implementation of consistent (CIFECM) boundaries for wave propagation problems in two-dimensional domains in ABAQUS using user-defined boundary element. Future work on consistent boundary implementation in three-dimensional continuum domain is a natural continuation of the present work.

Conflict of Interest

The authors confirm that there is no conflict of interest to declare for this publication.

Acknowledgements

The authors would like to express their sincere thanks to the editor and anonymous reviewers for their time and valuable suggestions.

References

Chen, X., Birk, C., & Song, C. (2014). Numerical modelling of wave propagation in anisotropic soil using a displacement unit-impulse-response-based formulation of the scaled boundary finite element method. *Soil Dynamics and Earthquake Engineering*, *65*, 243–255.

Emani, P. K., & Maheshwari, B. K. (2009). Dynamic impedances of pile groups with embedded caps in homogeneous elastic soils using CIFECM. *Soil Dynamics and Earthquake Engineering*, *29*(6), 963–973.

Emani, P. K., Kumar, R., & Vedula, P. (2016). Inelastic response spectrum for seismic soil pile structure interaction. *International Journal of Geotechnical Earthquake Engineering*, *7*(2), 24–34.

Gucunski, N., & Woods, R. D. (1992). Numerical simulation of the SASW test. *Soil Dynamics and Earthquake Engineering*, *11*(4), 213–227.

Lehmann, L., Langer, S., & Clasen, D. (2006). Scaled boundary finite element method for acoustics. *Journal of Computational Acoustics*, *14*(04), 489–506.

Liu, J., & Lin, G. (2012). A scaled boundary finite element method applied to electrostatic problems. *Engineering Analysis with Boundary Elements*, *36*(12), 1721–1732

Lin, G., Lu, S., & Liu, J. (2016). Transmitting boundary for transient analysis of wave propagation in layered media formulated based on acceleration unit-impulse response. *Soil Dynamics and Earthquake Engineering*, *90*, 494–509.

Maheshwari, B. K., & Emani, P. K. (2015). Three-dimensional nonlinear seismic analysis of pile groups using FE-CIFECM coupling in a hybrid domain and HISS plasticity model. *International Journal of Geomechanics*, *15*(3), 04014055.

Man, H., Song, C., Gao, W., & Tin-Loi, F. (2012). A unified 3D-based technique for plate bending analysis using scaled boundary finite element method. *International Journal for Numerical Methods in Engineering*, *91*(5), 491–515.

Ni, Y., Gu, W., & Shi, Z. (2022). A new artificial boundary condition for numerical simulation of elastic waves. *Soil Dynamics and Earthquake Engineering*, *152*, 107026.

Olsoninstruments. (2021). *Spectral analysis of surface waves, freedom data PC platform*. Retrieved from www.olsoninstruments.com.

Patchamatla, J. R. R., & Emani, P. K. (2020). Time domain implementation of transmitting boundaries in ABAQUS for discrete soil-structure interaction systems. *International Journal of Mathematical, Engineering and Management Sciences*, *5*(3), 447–462.

Poul, M. K., & Zerva, A. (2018). Time-domain PML formulation for modeling viscoelastic waves with Rayleigh-type damping in an unbounded domain: Theory and application in ABAQUS. *Finite Elements in Analysis and Design*, *152*, 1–16.

Saputra, A., Talebi, H., Tran, D., Birk, C., & Song, C. (2017). Automatic image-based stress analysis by the scaled boundary finite element method. *International Journal for Numerical Methods in Engineering*, *109*(5), 697–738.

Wolf, J. P. (2003). *The scaled boundary finite element method*. Chichester: John Wiley & Sons.

Wolf, J. P., & Deeks, A. J. (2004). *Foundation vibration analysis: A strength of materials approach*. Amsterdam: Elsevier.

Wolf, J. P., & Song, C. (1996). *Finite-element modelling of unbounded media*. Chichester: Wiley.

Wolf, J. P., & Song, C. (2000). The scaled boundary finite-element method—A primer: Derivations. *Computers & Structures*, *78*(1–3), 191–210.

Xing, H., Li, X., Li, H., & Liu, A. (2021). Spectral-element formulation of multi-transmitting formula and its accuracy and stability in 1D and 2D seismic wave modeling. *Soil Dynamics and Earthquake Engineering*, *140*, 106218.

Yang, Z. (2006). Fully automatic modelling of mixed-mode crack propagation using scaled boundary finite element method. *Engineering Fracture Mechanics*, *73*(12), 1711–1731.

Appendix-A

The following formulation of CIFECM are taken from (Wolf & Song, 1996)
Coefficient Matrices for three-dimensional vector wave equation

$$\left.\begin{aligned}
[E^0] &= \int_{-1}^{+1}\int_{-1}^{+1}[B^1]^T[D][B^1]|J|d\eta\, d\zeta \\
[E^1] &= \int_{-1}^{+1}\int_{-1}^{+1}[B^2]^T[D][B^1]|J|d\eta\, d\zeta \\
[E^2] &= \int_{-1}^{+1}\int_{-1}^{+1}[B^2]^T[D][B^2]|J|d\eta\, d\zeta
\end{aligned}\right\} \tag{8}$$

Where the strain displacement matrices $[B^1], [B^2]$ are obtained from the elements of Jacobian matrix as follows

$$[B^1]_k = \begin{bmatrix} j_{11} & 0 & 0 \\ 0 & j_{21} & 0 \\ 0 & 0 & j_{31} \\ 0 & j_{31} & j_{21} \\ j_{31} & 0 & j_{11} \\ j_{21} & j_{11} & 0 \end{bmatrix} N_k, \quad [B^2]_k = \begin{bmatrix} j_{12} & 0 & 0 \\ 0 & j_{22} & 0 \\ 0 & 0 & j_{32} \\ 0 & j_{32} & j_{22} \\ j_{32} & 0 & j_{12} \\ j_{22} & j_{12} & 0 \end{bmatrix} N_{k,\eta} + \begin{bmatrix} j_{13} & 0 & 0 \\ 0 & j_{23} & 0 \\ 0 & 0 & j_{33} \\ 0 & j_{33} & j_{23} \\ j_{33} & 0 & j_{13} \\ j_{23} & j_{13} & 0 \end{bmatrix} N_{k,\zeta} \tag{9}$$

The jacobian matrix is given by

$$[J] = \begin{bmatrix} \{N\}^T\{x\} & \{N\}^T\{y\} & \{N\}^T\{z\} \\ \{N_{,\eta}\}^T\{x\} & \{N_{,\eta}\}^T\{x\} & \{N_{,\eta}\}^T\{x\} \\ \{N_{,\zeta}\}^T\{x\} & \{N_{,\zeta}\}^T\{x\} & \{N_{,\zeta}\}^T\{x\} \end{bmatrix} \tag{10}$$

Where, the shape function $[N_k(\eta,\zeta)]$ are as follows

$$\left.\begin{aligned} N_1(\eta,\zeta) &= \tfrac{1}{4}(1-\eta)(1-\zeta) \\ N_2(\eta,\zeta) &= \frac{1}{4}(1+\eta)(1-\zeta) \\ N_3(\eta,\zeta) &= \frac{1}{4}(1+\eta)(1+\zeta) \\ N_4(\eta,\zeta) &= \frac{1}{4}(1-\eta)(1+\zeta) \end{aligned}\right\} \tag{11}$$

$$[m^\infty]_1^2 + \frac{\Delta t}{2}([e^1]+[I])[m^\infty]_1 + [m^\infty]_1\frac{\Delta t}{2}([e^1]^T+[I]) - \frac{\Delta t^2}{6}[e^2] - [m^0] = 0 \tag{12}$$

Where the coefficient matrices $[e^1], [e^2], [m^0]$ are given by

$$\left.\begin{aligned} [e^1] &= ([U]^{-1})^T[E^1][U]^{-1} - \frac{s+1}{2}[I] \\ [e^2] &= ([U]^{-1})^T([E^2]-[E^1][E^0]^{-1}[E^1]^T)[U]^{-1} \\ [m^0] &= ([U]^{-1})^T[M^0][U]^{-1} \end{aligned}\right\} \tag{13}$$

The unitary matrix $[U]$ is determined from coefficient matrix $[E^0]$

$$[E^0] = [U]^T[U] \tag{14}$$

$$\begin{aligned} &\left([m^\infty]_1 + \frac{\Delta t}{2}[e^1]\right)[m^\infty]_n + [m^\infty]_n\left([m^\infty]_1 + \frac{\Delta t}{2}[e^1]^T\right) + t[m^\infty]_n = \\ &-\sum_{j=2}^{n-1}[m^\infty]_{n-j+1}[m^\infty]_j - [e^1]\left(\frac{[J]_{n-1}}{\Delta t} + [I]_{n-1}\right) \\ &-\left(\frac{[J]_{n-1}}{\Delta t} + [I]_{n-1}\right)[e^1]^T + \frac{t^3}{6\Delta t}[e^2] + \frac{t}{\Delta t}([m^0]-[I]_{n-1}) \end{aligned} \tag{15}$$

Appendix- B

Coefficient Matrices for two-dimensional vector wave equation

$$\left.\begin{aligned} [E^0] &= \frac{2}{3}\begin{bmatrix} 2[Q^0] & [Q^0] \\ [Q^0] & 2[Q^0] \end{bmatrix} \\ [E^1] &= \frac{1}{3}\begin{bmatrix} -[Q^0] & [Q^0] \\ [Q^0] & -[Q^0] \end{bmatrix} + 2\begin{bmatrix} -[Q^1] & -[Q^1] \\ [Q^1] & [Q^1] \end{bmatrix} \\ [E^2] &= \frac{1}{3}\begin{bmatrix} [Q^0] & -[Q^0] \\ -[Q^0] & [Q^0] \end{bmatrix} + 4\begin{bmatrix} [Q^2] & -[Q^2] \\ -[Q^2] & [Q^2] \end{bmatrix} \\ [M^0] &= \frac{\rho a}{6}\begin{bmatrix} 2[I] & [I] \\ [I] & 2[I] \end{bmatrix} \end{aligned}\right\} \tag{16}$$

Where

$$\left.\begin{aligned} [Q^0] &= \frac{1}{4a}[C^1]^T[D][C^1] \\ [Q^1] &= -\frac{1}{4a}[C^2]^T[D][C^1] \\ [Q^2] &= \frac{1}{4a}[C^2]^T[D][C^2] \end{aligned}\right\} \tag{17}$$

With

$$[C^1] = \begin{bmatrix} \Delta_y & 0 \\ 0 & -\Delta_x \\ -\Delta_x & 0 \end{bmatrix}, \qquad [C^2] = \begin{bmatrix} \bar{y} & 0 \\ 0 & -\bar{x} \\ -\bar{x} & \bar{y} \end{bmatrix} \tag{18}$$

Where

$$\left.\begin{aligned} a &= x_1 y_2 - x_2 y_1 \\ \Delta_x &= x_2 - x_1 \\ \Delta_y &= y_2 - y_1 \\ \bar{x} &= \tfrac{1}{2}(x_2 + x_1) \end{aligned}\right\} \tag{19}$$

$$\bar{y} = \frac{1}{2}(y_2 + y_1)$$

Also the stress-strain matrix for isotropic material is

$$[D] = \begin{bmatrix} \lambda + 2G & \lambda & 0 \\ \lambda & \lambda + 2G & 0 \\ 0 & 0 & G \end{bmatrix} \tag{20}$$

The MATLAB code for implementing the procedure of Appendix B is given below

```
%% BE calculations Wolf and Song (1996)
 % Coefficient matrices for all elements
 D=[lam+2*G lam 0;lam lam+2*G 0;0 0 G];
 NNODE=size(NODE,1);NBDOF=NNODE*2;
 E0=zeros(NBDOF,NBDOF);E1=E0;E2=E0;M0=E0;
 for e=1:NELEM
    n1=ELEM(e,1);n2=ELEM(e,2);edof=[2*n1-1;2*n1;2*n2-1;2*n2];
    x1=NODE(n1,1);y1=NODE(n1,2);
    x2=NODE(n2,1);y2=NODE(n2,2);
    a=x1*y2-x2*y1;Delx=x2-x1;Dely=y2-y1;
    x_=0.5*(x1+x2);y_=0.5*(y1+y2);
    C1=[Dely 0;0 -Delx;-Delx Dely];
    C2=[y_ 0;0 -x_;-x_ y_];
   Q0= 1/4/a*C1'*D*C1;
   Q1=-1/4/a*C2'*D*C1;
   Q2=1/4/a*C2'*D*C2;
   e0=2/3*[2*Q0 Q0;Q0 2*Q0];
   e1=1/3*[-Q0 Q0;Q0 -Q0]+2*[-Q1 -Q1;Q1 Q1];
   e2=1/3*[Q0 -Q0;-Q0 Q0]+4*[Q2 -Q2;-Q2 Q2];
   m0=rho*a/6*[2*eye(2) eye(2);eye(2) 2*eye(2)];
   E0(edof,edof)=E0(edof,edof)+e0;
   E1(edof,edof)=E1(edof,edof)+e1;
```

```
  E2(edof,edof)=E2(edof,edof)+e2;
  M0(edof,edof)=M0(edof,edof)+m0;
end
U=chol(E0);
invU=inv(U);invE0=inv(E0);I=eye(NBDOF);
e1=transpose(invU)*E1*invU-(s+1)/2*I;
e2=transpose(invU)*(E2-E1*invE0*transpose(E1))*invU;
m0=transpose(invU)*M0*invU;
%% SOlving a continuous Riccati Equation obtained after time-discretization
A=-dt/2*(transpose(e1)+I);Q=dt^2/6*e2+m0;B=I;
[minf1,L,G_] = care(A,B,Q);
Minf1=transpose(U)*minf1*U;
In=dt*minf1;Jn=(dt^2)/2*minf1;
t3=(t.^3)/6/dt;
A=minf1+dt/2*e1;[V,S]=schur(A);
minf=zeros(NBDOF,NBDOF,N);Minf=minf;
```